PROCEEDINGS, Thirty-Seventh Workshop on Geothermal Reservoir Engineering
Stanford University, Stanford, California, January 30 - February 1, 2012
SGP-TR-194

# THE INFLUENCE OF RESERVOIR HETEROGENEITY ON GEOTHERMAL FLUID AND METHANE RECOVERY FROM A GEOPRESSURED GEOTHERMAL RESERVOIR

Esposito, Ariel and Augustine, Chad

National Renewable Energy Laboratory
1617 Cole Blvd.
Golden, CO, 80401, USA
e-mail: ariel.esposito@nrel.gov

## ABSTRACT

Geopressured geothermal reservoirs are characterized by high temperatures and high pressures with correspondingly large quantities of dissolved methane. In many cases, the reservoirs are comprised of multilayer systems of thin sandstones and thicker shales. Below the low permeability shale layers, large quantities of gas may have accumulated over time. Two methods utilizing reservoir simulation techniques have been used to estimate recoverability factors of geothermal brine and methane based on well log data from a specific reservoir in Texas. The first assumes a simplified reservoir that has three layers: upper shale, sandstone, and lower shale with the sandstone layer thickness equal to the net sandstone in the reservoir interval. The second method uses a detailed reservoir model that accounts for multiple sandstone and shale layering. This method includes 12 layers of sandstone or shale with the layer depths determined from a well log. These two methods are used to answer the question on the sensitivity of the results to the level of detail that is included in the reservoir model.

Based on a comparison of the recovery of fluid and methane from the detailed and simplified model, the influence of incorporating reservoir heterogeneity was determined. It was found that incorporating multiple thin layers of lower permeability sandstone can noticeably impact the results of the reservoir simulation. The heterogeneous model resulted in greater flow rates of both geothermal brine and total methane. Both models demonstrate that the geopressured geothermal reservoir is capable of producing hot geothermal fluid at flow rates over a long duration that are sufficient for electricity production from binary power plants. The results indicate that simplified models of geopressured geothermal reservoirs that approximate actual reservoir details can be applied to give a reasonable, albeit conservative, estimate of the recoverable resource over broad areas using generalized data sets.

## INTRODUCTION

In the Gulf Coast geopressured geothermal reservoirs are present at depths greater than 2,400 m and have reservoir pressure gradients of 15.83 kPa/m and greater (Bebout et al., 1982). The formation of geopressured reservoirs is most often the result of compaction phenomena. When newly deposited sediments are overlain by younger sediments and burial begins, the pressure of the rock overburden increases and attempts to reduce the porosity and thickness of the deeper sediments. The ability of the buried sediment to expel the fluid to allow for a volumetric decrease is highly dependent on the permeability of the overlying rocks. If the overlying layers are fine-grained with very high entry pressure and low permeability, little fluid will be expelled and the fluid will bear some of the overburden, leading to a pressure increase up to the lithostatic pressure gradient of 22.62 kPa/m. Other overpressuring mechanisms include clay dehydration which leads to water influx and hydrocarbon maturation and results in increases in fluid volume and decreases in density.

Due to the reduction in fluid movement between layers and the lower thermal conductivity resulting from the higher porosity, the fluid temperatures in geopressured formations tend to be high, leading to thermal expansion. The mechanisms that lead to overpressuring occur over long geologic timescales, resulting in reservoirs at reasonably steady state conditions. The extent of the geopressured geothermal resource in the Gulf Coast of Texas is well documented by multiple previous studies that rely on an abundance of reservoir data that has been acquired by oil and gas exploration and production over the past century. The first assessment of onshore geopressured geothermal in the Gulf Coast region of Texas and Louisiana was completed by the U.S. Geological Survey (USGS) in 1975 (Papadopulos et al., 1975). In 1978, the USGS updated the previous assessment to include the offshore geopressured geothermal resources for both Texas and Louisiana

and incorporated thousands of data points from individual well cores and fluid chemistry measurements (Wallace et al., 1978). After this point multiple follow up studies were completed focusing on the gulf coast geopressured resource (Bebout et al., 1982; Bebout et al., 1983).

## METHODOLOGY

To analyze the production of hot geothermal fluid and methane from the reservoir of interest, reservoir modeling and simulation was used. Reservoir modeling and simulation allow for a detailed analysis of fluid production based on the main reservoir characteristics that influence flow. One major benefit of advances in reservoir simulation is the inclusion of complex multiphase flow dynamics that are dependent on pressure and temperature changes during the production period. TOUGH2 (Pruess et al., 1999) with the Equation-of-State for Water, Salt, and Gas (EWASG) was used to analyze the geopressured geothermal reservoir of interest (Battistelli et al., 1997). The EWASG module was implemented with $H_2O$, NaCl, and $CH_4$ as the three constituents. Also included in the reservoir simulation were relative permeability, capillary pressure, rock compressibility, and permeability anisotropy with the ratio of horizontal to vertical permeability ($k_r/k_z$) equal to 10 in both sand and shale.

For this study, three reservoir models were developed to understand the importance of reservoir detail on the results. The first, the heterogeneous reservoir model, is based on well log data from 2003 for an abandoned gas well in the Wilcox Formation in Goliad County, Texas. Analysis of the well log data showed four major producing zones between the depths of 3,475 m and 4,195 m. Each of the top three production zones were split into one sandstone and one shale layer based on the net-to-gross ratio that was determined by including sandstone with a minimum porosity of 6% and a maximum shale volume of 20%. The permeability and porosity for the net zones was calculated from averaging the well log data for those sections.

For the lowest producing interval, the shale layer was broken into two layers to match the well log data more closely. The total net sandstone thickness from the data is 173 m, which was rounded up to 180 m for the heterogeneous model due to rounding of the vertical thickness of the grid cells to reduce the total number of z layers and hence the total number of grid cells. Based on the well log data from 2003, between each producing zone, there is a low permeability shale layer that acts to reduce fluid movement between the layers. These low permeability shale layers help to maintain the overpressure in the reservoir. Figure 1 is a cross section view of the reservoir model depicting the multiple reservoir layers. Figure 2 shows the permeability with depth on a log scale for the heterogeneous model. Table 1 lists the layer properties for all seven layers in the heterogeneous model.

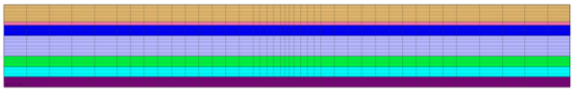

*Figure 1: Cross section view of the heterogeneous model showing the multiple reservoir layers*

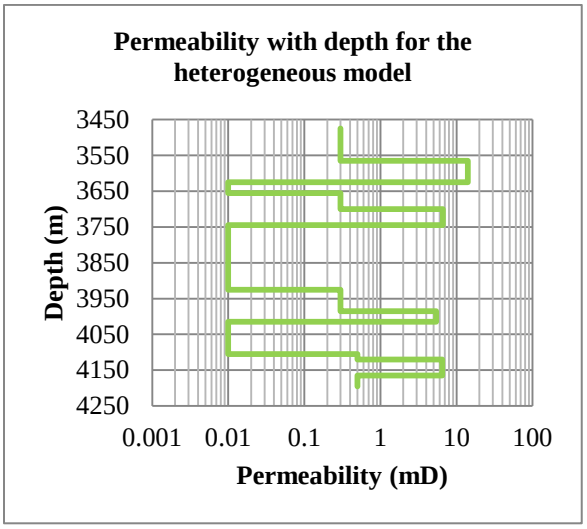


*Figure 2: Permeability profile with depth for Heterogeneous model*

*Table 1: Heterogeneous Model Layer Properties*

| | Layer | Sand/ Shale | Porosity | $k_r$ (mD) | Thickness (m) |
|---|---|---|---|---|---|
| Interval 1 | Layer 1 | Shale | 0.148 | 0.3 | 90 |
| | Layer 1 | Sand | 0.148 | 14.1 | 60 |
| | Layer 2 | Shale | 0.1385 | 0.01 | 30 |
| Interval 2 | Layer 3 | Shale | 0.129 | 0.3 | 45 |
| | Layer 3 | Sand | 0.129 | 6.6 | 45 |
| | Layer 4 | Shale | 0.125 | 0.01 | 180 |
| Interval 3 | Layer 5 | Shale | 0.121 | 0.3 | 60 |
| | Layer 5 | Sand | 0.121 | 5.4 | 30 |
| | Layer 6 | Shale | 0.123 | 0.01 | 90 |
| Interval 4 | Layer 7 | Shale | 0.125 | 0.5 | 15 |
| | Layer 7 | Sand | 0.125 | 6.5 | 45 |
| | Layer 7 | Shale | 0.125 | 0.5 | 30 |

The highest permeability sandstone is the sandstone layer in Layer 1 at 14.1 mD. This permeability is lower than the 20 mD sandstone permeability cutoff considered for a study of prospective geopressured

geothermal fairways in Texas (Bebout et al., 1982; Bebout et al., 1983). Because porosity data is not available for the low permeability shale layers, (Layer 2, Layer 4, and Layer 6), the average of the porosity of the layers above and below was used.

**Homogeneous reservoir models**

In addition to the heterogeneous model, two simplified reservoir models were developed. These models were developed to help quantify the influence of including the multiple layers of sandstone and shale in the reservoir model on the reservoir productivity. Also, they can help to determine if more detailed modeling is necessary to generate reasonable production results. These upscaled models are referred to as the homogeneous models because they only have one sandstone layer with consistent properties throughout and two shale layers.

There are multiple methods available to upscale from a set of detailed data to develop a reservoir model. The most important step in many cases is to determine the upscaled effective vertical ($k_z$) and horizontal permeability ($k_r$) that most closely match the detailed data. Three different averaging techniques are often used: the arithmetic mean, the harmonic mean, and the geometric mean. Conventionally, the harmonic mean or geometric mean is used to average the vertical permeability, which is the permeability in the direction that is perpendicular to the bedding (Weber and van Geuns, 1990). The geometric mean is most often used to determine the effective permeability for random, uncorrelated, and isotropic permeability distributions (Warren and Price, 1961). Based on the detailed data, the reservoir fits more closely with a simple stratified model in which case the harmonic mean permeability is more appropriate. However, because the layers are of unequal thickness, the weighted harmonic mean permeability was used (Eq. 1). In Equation 1, the weight, $w_i$, is the thickness of layer i, and $x_i$ is the vertical permeability of that layer.

$$\sum_{i=1}^{n} w_i \Big/ \sum_{i=1}^{n} \frac{w_i}{x_i} \qquad \textit{Eq. 1}$$

It is most common to use the arithmetic mean to determine the effective horizontal permeability, which is the permeability in the direction parallel to the bedding (Weber and van Geuns, 1990). However, because the permeability values among the shale layers varies by a magnitude of more than 10 in some cases, the arithmetic mean will be strongly biased towards the thinner and higher permeability shale layers. For this reason, the weighted harmonic mean was also used to determine the effective horizontal permeability as a more unbiased estimate. Because the same upscaling method of the weighted harmonic mean was used for both the vertical and horizontal permeability, the anisotropy ratio of $k_r/k_z=10$ was maintained in both the homogeneous and heterogeneous models. The sandstone and shale porosity for the homogeneous models was upscaled using the arithmetic mean because the values between each layer are very similar (Table 1).

A final aspect to determine as part of the upscaling is the relative placement of the sandstone and shale layers within the reservoir thickness. Based on the data, in the top 270 m of the reservoir, there is 100 m of sandstone; in the lower 210 m of the reservoir, there is 72 m of sandstone, with a gap of 240 m of shale in the middle. Because it is not evident whether placing the sandstone closer to the top or closer to the bottom of the reservoir more accurately upscales the data, two models were developed with two different sandstone placements. For both cases the sandstone thickness was rounded to a total of 175 m. The first, with the cross section view shown in Figure 3, has the sandstone placed at a shallower depth (Homogeneous Shallow). The upper shale layer is comprised of shale from Layer 1 through Layer 3. The lower shale layer is comprised of the shale from Layer 4 through Layer 7. Table 2 lists the properties for the three layers for the homogeneous model with the shallow sandstone.

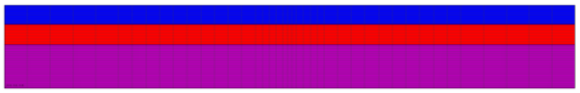

*Figure 3: Cross section view of the homogeneous model with the shallow sandstone layer*

*Table 2: Layer properties for the homogeneous model with shallow sandstone layer*

| | Layer | Porosity | $k_r$ (mD) | Thickness (m) |
|---|---|---|---|---|
| | Upper Shale | 0.138 | 0.0478 | 165 |
| Interval 1 | Sand | 0.131 | 7.70 | 175 |
| | Lower Shale | 0.123 | 0.0139 | 380 |

The second homogeneous model (Homogeneous Deep) has the sandstone layer at a depth 180 m deeper. The upper shale layer is comprised of shale from Layer 1 through Layer 4 and the lower shale layer is comprised of shale from Layer 5 through Layer 7. By combining different initial shale layers for the upper and lower shale layers in the two homogeneous models, the permeability's of the upper and lower shale layers varies between the models. Figure 4 shows the cross section view of the Homogeneous Deep reservoir and Table 3 lists the layer properties. The sandstone layer properties are the same between each homogeneous model because

it is comprised of the same layers in both cases. The permeability of the upper shale is significantly lower for the case with the deeper sandstone layer because of the inclusion of more low permeability shale in that section.

*Figure 4: Cross section view of the homogeneous model with the deep sandstone layer*

*Table 3: Layer properties for the homogeneous model with the deep sandstone*

| | Layer | Porosity | $k_r$ (mD) | Thickness (m) |
|---|---|---|---|---|
| | Upper Shale | 0.135 | 0.0161 | 345 |
| Interval 1 | Sand | 0.131 | 7.70 | 175 |
| | Lower Shale | 0.123 | 0.0215 | 200 |

Figure 5 shows the permeability with depth on a log scale for the two homogeneous models. This figure clearly shows the difference in depth of the sandstone between the two models and how the permeability of the upper and lower shale changes between the models.

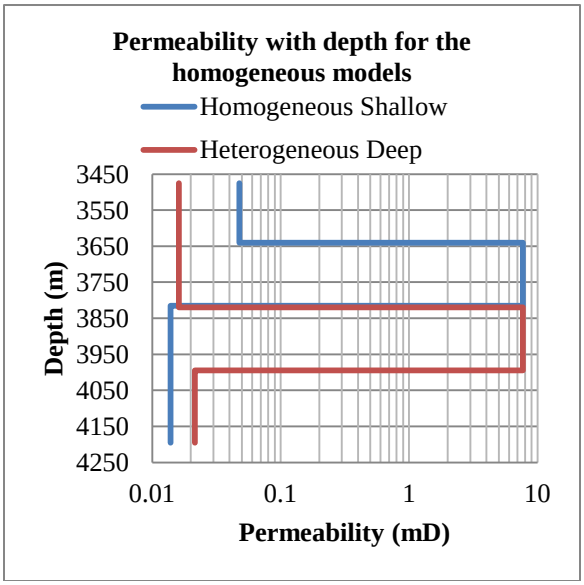


*Figure 5: Permeability with depth for the two homogeneous models*

**Reservoir properties:**

***Reservoir Volume:***

One area where there is uncertainty for the reservoir of interest is the reservoir volume based on the distance to impermeable faults. Different distances between parallel impermeable faults were considered to understand the influence of reservoir volume on flow rate. The reservoir was assumed to have a square planar geometry. For each model, three different distances (d) between the two sets of parallel impermeable boundaries were considered: d = 5 km (Case 1), d = 7.1 km (Case 2), and d = 10 km (Case 3). This corresponds to a reservoir volume of 18 $km^3$ for Case 1, 36 $km^3$ for Case 2, and 72 $km^3$ for Case 3.

***Pressure:***

The bottom hole pressure measurement of 65.5 MPa at 4,195 m equates with a pressure gradient of 15.61 kPa/m. This pressure gradient is very close to hard geopressure which was defined by the Bureau of Economic Geology at 15.83 kPa/m (Loucks et al., 1981). Figure 6 shows the stabilized reservoir pressure for all three models after an initialization period of 100 years. The reservoir model is run for 100 years to create a steady state condition before production begins. Due to the variation in the layering and the location of the sandstone and shale, the stabilized reservoir pressure is not the same between all three models.

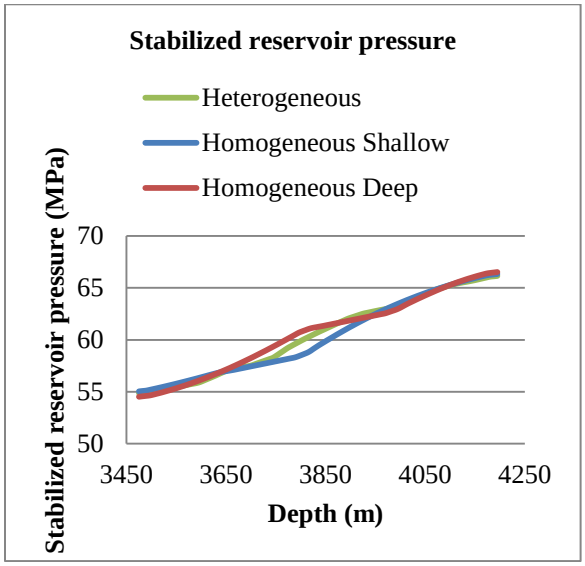


*Figure 6: Stabilized reservoir pressure for the three models*

***Temperature:***

The temperature measurements fit a straight line through the reservoir with a gradient of 5.25°C/100 m with a minimum temperature of 151.7°C at the top and a maximum of 186.7°C at the bottom.

***Gas saturation:***

A gas saturation of 1% was measured during the well log analysis in the upper producing layer. Based on this, the gas saturation based on a percent of the pore volume filled with free phase methane was set to 1%

throughout the entire interval. More gas is present in layers with higher porosities than in layers with lower porosity.

***Pore compressibility:***

A pore compressibility factor of $9x10^{-9}$ $Pa^{-1}$ was included to account for pore volume changes with changes in reservoir pressure. The pore compressibility factor is based on laboratory data for unconsolidated sands and is higher than the pore compressibility factors for consolidated sands (Yale et al., 1993). The unconsolidated characteristic of geopressured reservoirs in the Gulf Coast is clearly documented based on significant sand production during geopressure geothermal design well operations (Riney, 1988; Riney, 1991).

***Relative permeability:***

The relative permeability curves used were constant for all layers and are shown in Figure 7 with the green line corresponding to gas and the purple to water. These are representative curves based on the van Genuchten- Mualem (1980) model for relative permeability and are not from core data. The residual gas saturation was set to 5% and the irreducible water saturation was set to 25%.

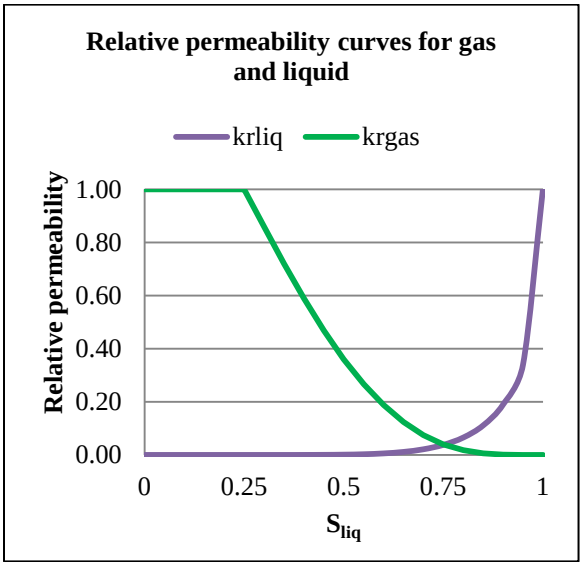


*Figure 7: Relative permeability curves for gas and liquid*

***Capillary pressure:***

The capillary pressure curves are representative curves by rock type that are based on the van Genuchten (1980) model for capillary pressure and are not from core data. The capillary pressure curve varied between the shale and the sandstone layers. Figure 8 shows the capillary pressure curves with the blue lines corresponding to shale and the red corresponding to sandstone. The capillary pressure is inversely correlated with pore throat diameter, where a much higher capillary pressure for shale corresponds with a much lower pore throat diameter in the shale (Schowalter and Hess, 1982).

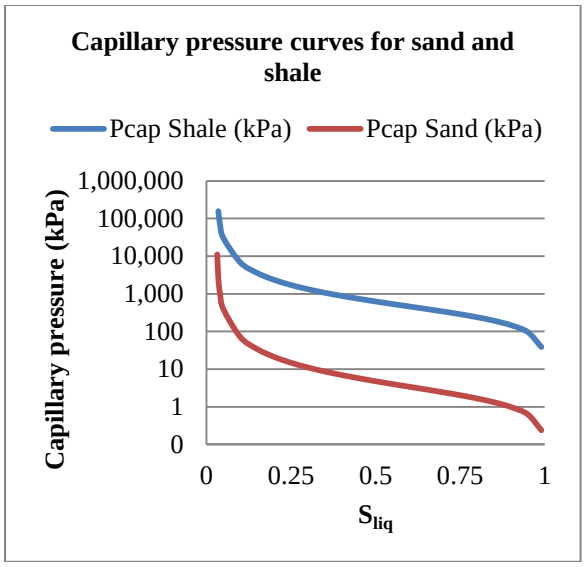


*Figure 8: Capillary pressure curves for sand and shale*

***Salinity:***

There were no salinity measurements available in the depth of interest. However, at a shallower depth a measurement of 82,300 ppm was taken. Due to the inherent error in extrapolating this value downward, a value of 80,000 ppm was used. Salinity measurements at the depth of interest in nearby wells in geopressured formations are close to the 80,000 ppm used for this analysis (Gregory et al., 1980).

**<u>Production well properties</u>**

For all cases, the production well is located in the center of the reservoir. The well diameter of 14 cm is also constant in all cases. The location of the screened well region varies between the heterogeneous case and the homogeneous cases. For the heterogeneous cases, the well is screened for a total of 180 m spread out over each sandstone layer. The homogeneous cases have the well screened for 175 m throughout the single sandstone interval. For the heterogeneous reservoir model, the top of the screened section is at 3,565 m, for the Homogeneous Shallow model it is at 3,640 m, and for the Homogenous Deep model it is at 3,820 m.

The well is operated with a constant pressure constraint with time to allow for variable flow between the different sandstone grid cell layers. To fully understand the influence of pressure on fluid production, different pressure constraints are

implemented for Run A, Run B, and Run C. The pressure at the top of the screened section, at the top of the well, and the initial pressure differential between the top of the screened section and the reservoir for the different model runs is listed in Table 4. The well head pressure is calculated assuming a hydrostatic gradient of 10.37 kPa/m in the well based on a fluid density that includes the 80,000 ppm NaCl salinity assumption.

*Table 4: Pressure at the top of the screened section, at the well head, and the initial pressure differential for the three different reservoir models for three different scenarios*

| **Pressure at top of screened section** | | | |
|---|---|---|---|
| **Run** | Heterogeneous | Homogeneous Shallow | Homogeneous Deep |
| **A** | 40 MPa | 40 MPa | 40 MPa |
| **B** | 40 MPa | 40.8 MPa | |
| **C** | | 40 MPa | 44.2 MPa |
| **Pressure at the top of the well** | | | |
| **Run** | Heterogeneous | Homogeneous Shallow | Homogeneous Deep |
| **A** | 3.0 MPa | 2.2 MPa | 0.4 MPa |
| **B** | 3.0 MPa | 3.0 MPa | |
| **C** | | 2.2 MPa | 4.6 MPa |
| **Initial pressure differential between well and reservoir** | | | |
| **Run** | Heterogeneous | Homogeneous Shallow | Homogeneous Deep |
| **A** | 15.6 MPa | 16.9 MPa | 21.1 MPa |
| **B** | 15.6 MPa | 16.1 MPa | |
| **C** | | 16.9 MPa | 16.9 MPa |

For Run A, the pressure at the top of the screened interval is the same for all reservoir models. This leads to a final pressure at the top of the sandstone layers after production that is similar for all reservoir models. For Run B, the pressure at the well head is the same between the Heterogeneous and the Homogenous Shallow reservoir models. Keeping the well head pressure equal between the two cases mimics operating the well in the same manner. For Run C, the pressure differential between the reservoir and the top of the screened well section is the same for Homogeneous Shallow and Homogeneous Deep. With the pressure differential equal, the influence of this parameter on the flow rate can be determined. Comparing results among the three runs allows for the impacts of the assumed well pressure to be separated from the influence of the structure and location (depth) of the sandstone intervals among the different models.

The well productivity index, which is based on the permeability of the reservoir, the length of the well, and the diameter of the well, was calculated for the Heterogeneous model and set to be constant for all other cases at $3.75 \times 10^{-12}$ $m^3$ (Coats, 1977). The well was operated for a period of 30 years to correspond with the planned lifetime of a small binary power plant. Operating the well over a long-term time frame provides insights on the influence of the exsolution of methane from the fluid on the total methane produced.

## RESULTS

The total mass flow rate of methane and geothermal fluid combined and the gaseous methane flow rate vary the most between the different models (Heterogeneous, Homogeneous Shallow, and Homogeneous Deep), the different reservoir volumes based on different distances between parallel reservoir boundaries (Case 1, Case 2, and Case 3), and the different model runs (Run A, Run B, and Run C).

The majority of the mass flow is fluid with less than 0.1% of the mass in gaseous phase. However, the density of gas is approximately 28% of the fluid density at the high pressures in the reservoir and continues to drop as the fluid reaches the surface. Hence, by volume the gas corresponds to a much greater percentage of the flow rate as it rises in the well. The aqueous phase methane flow rate tracks the fluid flow rate closely because the aqueous phase mass fraction only decreases by about 1.5% over the 30-year production period due to the drop in pressure in the reservoir from production.

### Total flow rate

The total fluid flow rate is primarily controlled by the difference between the initial reservoir pressure and the well pressure constraint and by the amount that the reservoir pressure declines with time which varies between the homogeneous and heterogeneous models. Figure 9 shows the total fluid flow rate for Run A with constant pressure at the top of the screened section for Case 1 (d = 5 km) for all three reservoir models.

At all times, the total flow rate is higher in the Heterogeneous model than for the two models with the homogeneous sandstone. The lower flow rate for Homogeneous Shallow compared with Homogeneous Deep is primarily due to the greater difference between the initial reservoir pressure and the constant pressure in the well for Homogeneous Deep for Run A. However, the flow rate for the Homogeneous Deep declines at a faster rate than all other cases. This is most likely a result of the very high initial pressure differential between the reservoir and the well.

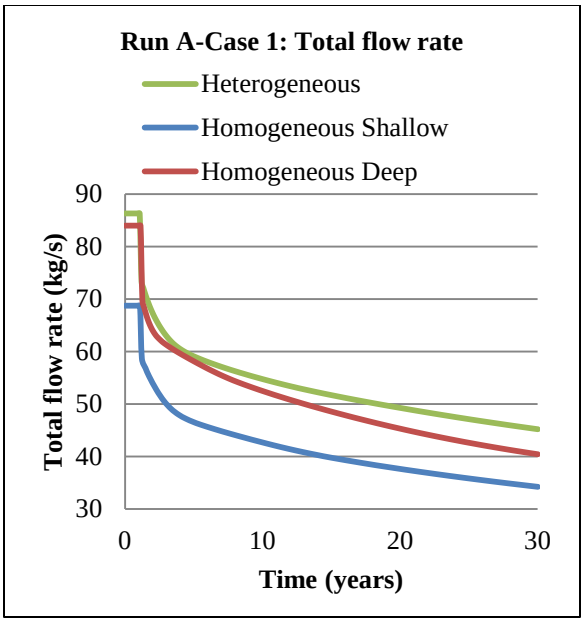


*Figure 9: Total flow rate for Run A for Case 1 (d=5 km) for all three reservoir models*

If the wells are operated at the same initial well head pressure as in Run B, then the difference in total flow rate between the Heterogeneous model and the Homogeneous Shallow model is even greater. This is because the fluid flow rate drops slightly due to a smaller initial pressure differential between the well and reservoir in the Homogeneous Shallow case for Run B. This can be seen in Figure 10 by the greater difference between the Heterogeneous total flow rate and the Homogeneous Shallow flow rate for Run B with the same well head pressure.

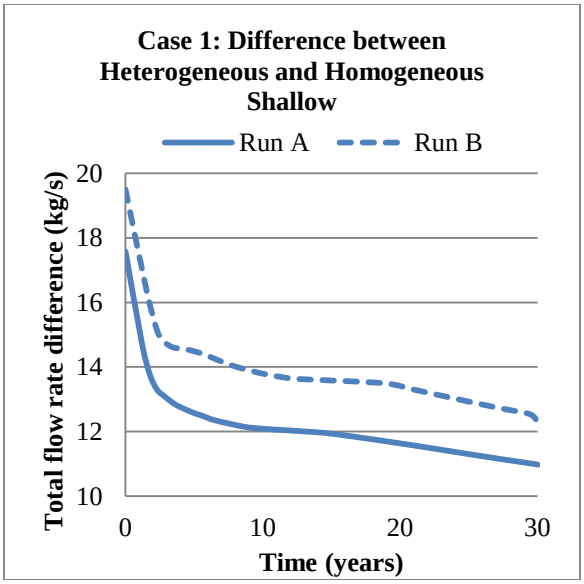


*Figure 10: Difference in the total flow rate between the Heterogeneous and Homogeneous Shallow models for Run A and Run B*

Figure 11 shows the total flow rate for Run C, where the Homogeneous Deep and Homogeneous Shallow models are operated with the same pressure differential. The total fluid flow rate over time is very similar between the two cases with a slight difference at the beginning. The results from Run C show that the most important factor controlling flow rate in the well for the homogeneous models is the initial difference between the reservoir pressure and the well pressure at the top of the screened section. It can be assumed that if this difference is removed for the other cases, then the results between the Homogeneous Shallow and Homogeneous Deep will be quite similar.

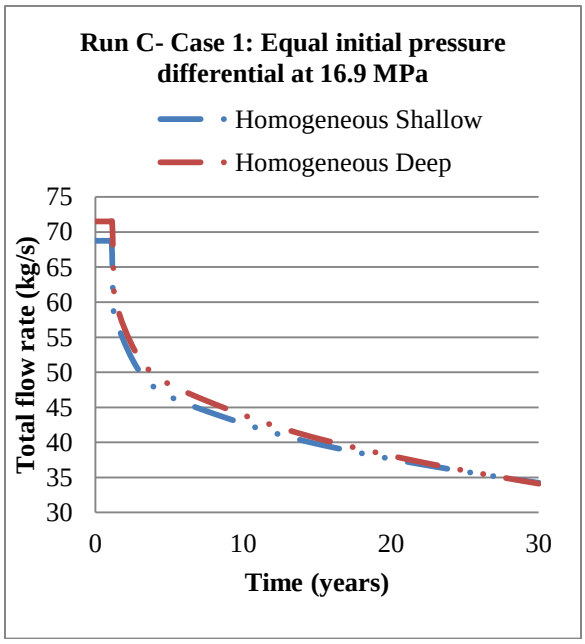


*Figure 11: Total flow rate for the Homogeneous Deep model run at 44.2 MPa and the Homogeneous Shallow run at 40 MPa*

**Influence of reservoir volume**

To understand the influence of the reservoir volume on production, the Homogeneous Shallow model and the Heterogeneous model were run for all three different reservoir volumes corresponding to different distances between the barriers: Case 1 (d=5 km), Case 2 (d=7.1 km), and Case 3 (d=10 km). The distance from the well to the impermeable boundary corresponds to half the distance between the two boundaries because the well is placed in the center of the square reservoir. For Case 1 the well is 2.5 km from any boundary, Case 2 it is 3.55 km from any boundary, and Case 3 it is 5 km from any boundary.

***Homogeneous Shallow***

Figure 12 shows the total flow rate over time for all three cases for the Homogeneous Shallow model.

When the distance to the impermeable boundary increases, the total flow rate after the first five years of production also increases. The difference between Case 2 and Case 3 is much smaller than between Case 1 and Case 2. This clearly shows that as the distance to the boundary is increased, the impact of the boundary on the flow rate decreases and may eventually reach a point where the influence of the boundary is negligible.

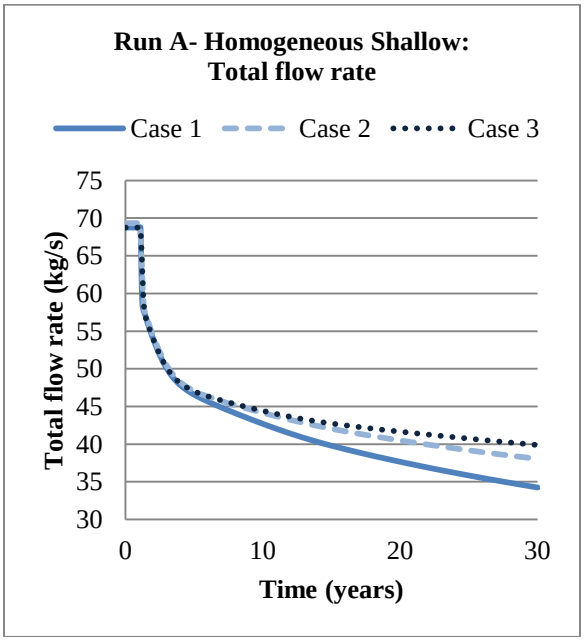


*Figure 12: Total flow rate for the Homogeneous Shallow model for all three cases*

***Heterogeneous***

Figure 13 shows the total flow rate for all three cases for the Heterogeneous model. The difference between the three cases is similar to the Homogeneous Shallow results (Figure 12). The final flow rate between the three cases for the Heterogeneous model spans from 45 kg/s for Case 1 to 49.5 kg/s for Case 3—a difference of 4.5 kg/s. The difference between the final flow rate for Case 1 and Case 3 with the Homogeneous Shallow model is slightly higher at 5.75 kg/s. Based on these results we can conclude that having separate layers of sandstone in the Heterogeneous model reduces the impact of the reservoir boundary on the total flow rate, discussed below. The total flow rate for all of the Heterogeneous cases is higher at all times by approximately 15 kg/s compared with the Homogeneous Shallow model.

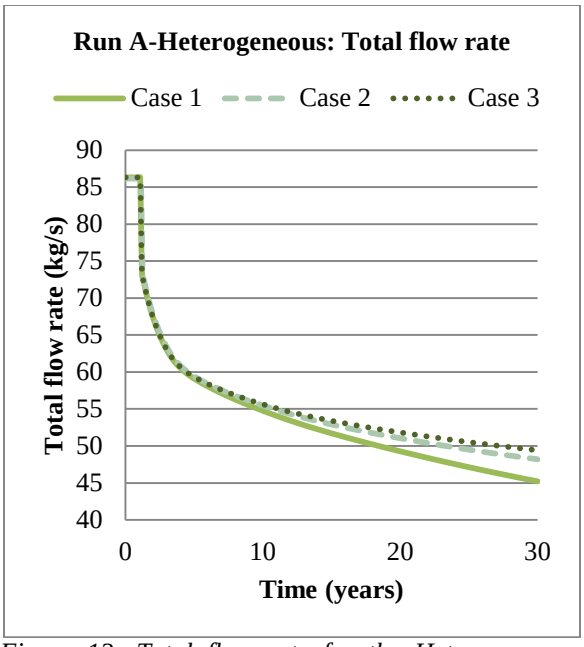


*Figure 13: Total flow rate for the Heterogeneous model for all three cases for Run A*

**Gaseous methane flow rate**

Another relevant comparison between the different reservoir models and the different reservoir volumes is the gaseous methane flow rate. This flow rate corresponds to the amount of gas flowing in the screened portion of the well. The mass fraction of methane in the gas phase compared to the aqueous phase may increase as the fluid rises to the surface. While the fluid rises to the surface, the pressure in the well declines and the maximum aqueous phase concentration decreases leading to the exsolution of dissolved methane.

Changes in the gaseous methane flow rate in the screened portion of the well with time are a result of exsolution of gaseous methane from the fluid, changes in reservoir pressure, and total fluid flow. Because the fluid is fully saturated with methane at all times, any drop in pressure in the reservoir corresponds with an increase in the gaseous phase methane. Due to the trapping of the gas bubbles in the pores, which is accounted for by a residual gas saturation of 5% in the relative permeability curves, methane is only mobile at gas saturations greater than 5%. Figure 14 shows the gaseous flow rate for all three models for Case 1 (d=5 km).

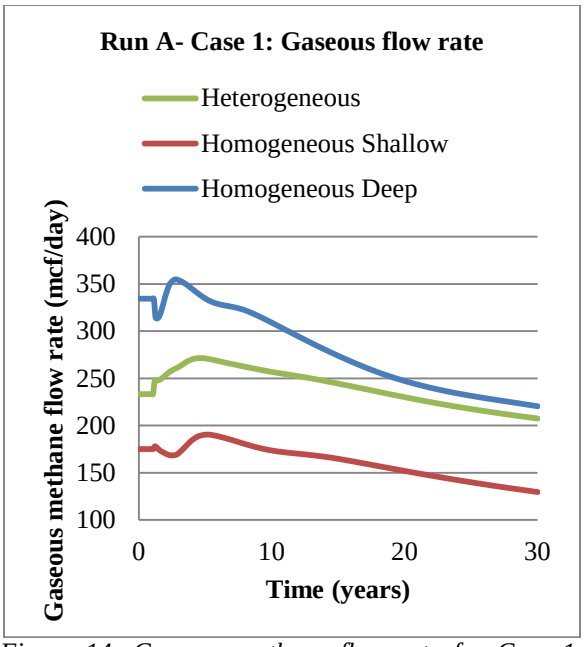


*Figure 14: Gaseous methane flow rate for Case 1 (d=5 km) for all three models for Run A*

The gaseous methane flow rate results do not follow the same trend as the total flow rate. At all times the Homogeneous Deep model has a higher gaseous methane flow rate than all other model runs. The gaseous flow rate decline is also the highest for the Homogeneous Deep model. These two factors are due to the large initial pressure differential between the well and the reservoir for the Homogeneous Deep case presented here. Because the pressure drops so significantly quite quickly after the well begins production, the amount of methane that exsolves from the fluid is quite high. This gaseous methane is close to the well and is produced first. However, after the initial high production of this gaseous methane, the remaining methane is at lower gas saturation and follows the gaseous flow rate decline rate of the Heterogeneous and Homogeneous Shallow models.

Similar to the total fluid flow rate, the Homogeneous Shallow has a significantly lower flow rate of gaseous methane than the other two models presented here. If the Homogeneous Deep model is run with the higher well pressure of 44.2 MPa instead of 40 MPa, the gaseous methane flow rate is still slightly higher than the Homogeneous Shallow model even though the initial pressure differential is the same. The reason for the slight difference is that even though the initial pressure differential is the same between the two models, the reservoir pressure drops more rapidly for the Homogeneous Deep model producing a slightly higher amount of exsolved gas.

***Homogeneous Shallow:***

For the Homogeneous Shallow model, the distance to the impermeable boundary has a significant influence on the gaseous methane production, which is clearly shown in Figure 15. The gaseous methane flow rate for each case is quite similar up until 5 years of production. After this time, the gaseous methane flow rate declines significantly for Case 1 with the closest reservoir boundary at 2.5 km away. The decline rate for Case 3 with the greatest distance to the boundary is much slower, dropping from 192 mcf/day to 175 mcf/day as compared with a drop from 190 mcf/day to 128 mcf/day for Case 1. The rapid decline rate for Case 1 is likely because the relative reservoir volume significantly influenced by the pressure drop in the well is impacted much sooner in time than for Case 2 and Case 3 with correspondingly larger reservoir volumes.

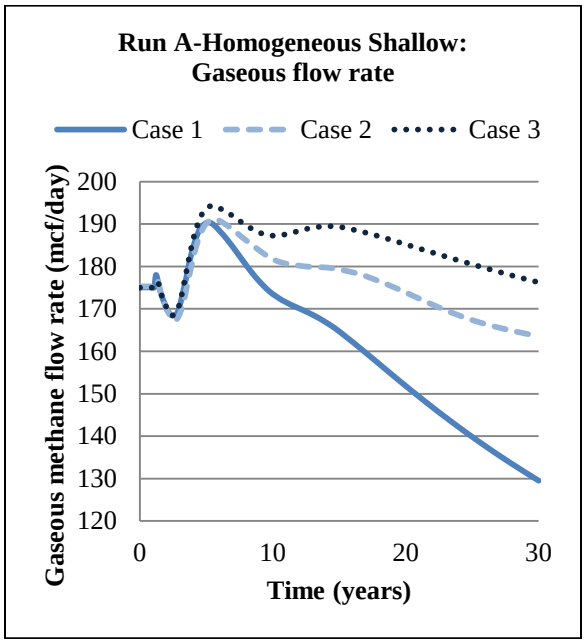


*Figure 15: Gaseous methane flow rate for the Homogeneous Shallow model for all three cases for Run A*

***Heterogeneous:***

In comparison, for the Heterogeneous model, the gaseous methane flow rate for all the three cases is much higher over time than for the Homogeneous Shallow model (Figure 16). Also, the gaseous methane flow rates between the three cases are very close up until 10 years. In addition, the initial increase in gaseous methane flow is much higher for the Heterogeneous model than for the Homogeneous Shallow model, jumping from 233 mcf/day to 272 mcf/day over a short time. The gaseous methane flow rates for Case 2 and Case 3 never drop back below the initial 233 mcf/day. The

slight increase in gaseous methane flow rate at 13 years observed for Case 2 and Case 3 in the Homogeneous Shallow model is not as pronounced in the Heterogeneous model flow rate for those cases. For this reason, the drop between the high gaseous methane flow rate at 3.5 years and the final gaseous methane flow rate at 30 years is about 30 mcf/day for both Case 2 and Case 3, greater than the drop in the Homogenous Shallow cases.

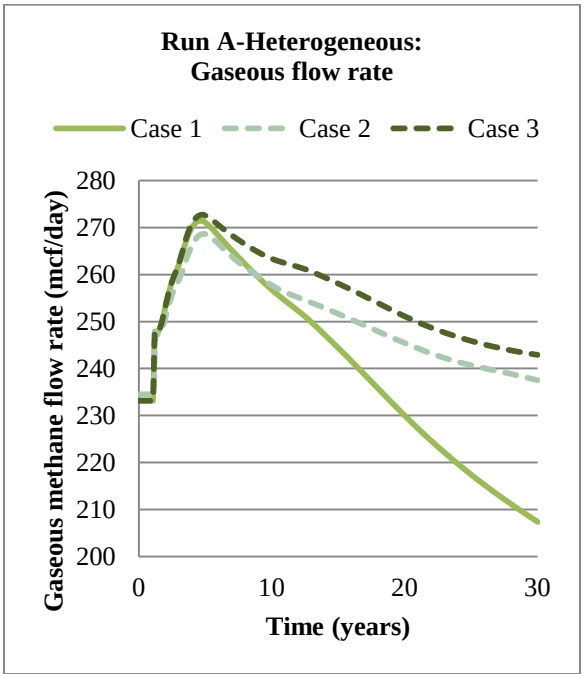


*Figure 16: Gaseous methane flow rate for the Heterogeneous model for all three cases for Run A*

**Result summary**

Table 5 lists the summary values for all three cases for the Homogenous Shallow model and the Heterogeneous model presented here. The most important summary simulation output values are the average total flow rate and the total heat recovered in terms of joules with a reference temperature of 25 °C from the geothermal fluid alone. Also listed in Table 5 is the total methane produced over the 30-year production period accounting for both the aqueous and gaseous phase methane for all three cases. To sell this methane, any remaining aqueous phase methane would need to be separated from the geothermal fluid at the surface.

*Table 5: Summary values for the Homogeneous Shallow and Heterogeneous models for all three cases for Run A*

| **Run A- Homogeneous Shallow** | | | |
|---|---|---|---|
| | Avg flow rate (kg/s) | Total heat recovered (J) | Total methane recovered (BCF) |
| **Case 1** | 41.4 | $1.18 \times 10^{16}$ | 11.5 |
| **Case 2** | 43.5 | $1.23 \times 10^{16}$ | 12.2 |
| **Case 3** | 44.3 | $1.24 \times 10^{16}$ | 12.5 |
| **Run A- Heterogeneous** | | | |
| | Avg flow rate (kg/s) | Total heat recovered (J) | Total methane recovered (BCF) |
| **Case 1** | 53.7 | $1.56 \times 10^{16}$ | 16.4 |
| **Case 2** | 55.1 | $1.59 \times 10^{16}$ | 16.9 |
| **Case 3** | 55.6 | $1.59 \times 10^{16}$ | 17.0 |

**DISCUSSION**

For all cases for both the Homogeneous Shallow model and the Heterogeneous model, as the distance to the impermeable boundary increases, all of the summary values presented in Table 5 increase. The total methane recovered for Case 2 and Case 3 for the Heterogeneous model are very similar. However, from Figure 16 it is clear that the gaseous methane flow rate over time does vary between these two cases. The difference in gaseous methane flow rate shown in Figure 16 does not have a significant impact when calculating the total amount of methane recovered. This is because the majority of the methane produced is in aqueous phase at the reservoir conditions. Figure 17 shows the total flow rate, the aqueous phase methane flow rate, and the gaseous phase methane flow rate for Run A in the Heterogeneous model for Case 1. The distribution where most of the methane is produced in aqueous phase is similar across the cases and model runs.

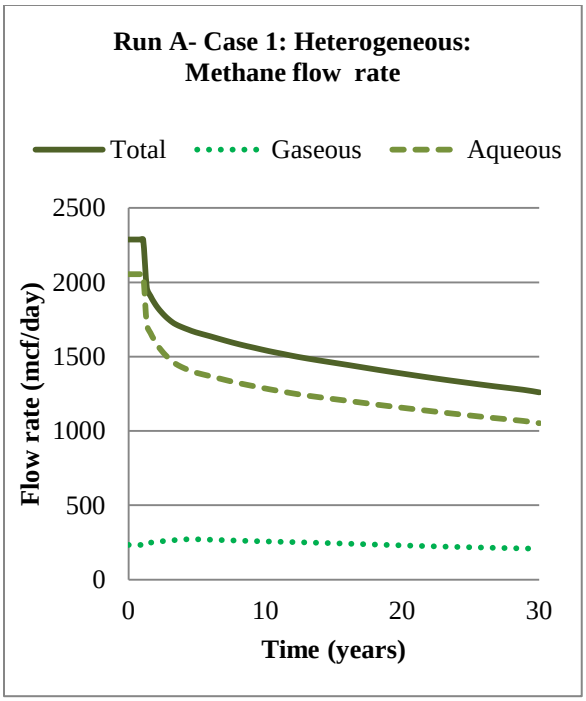


*Figure 17: Methane flow rate breakdown for Case 1 for the Heterogeneous model for Run A*

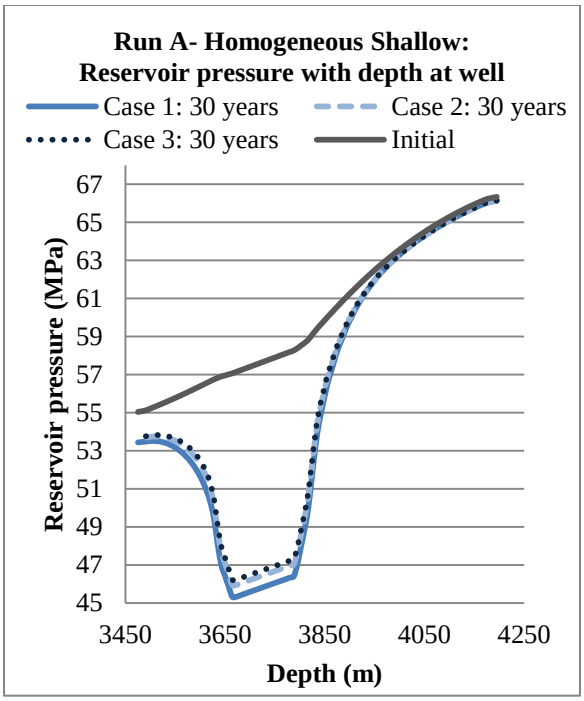


*Figure 18: Reservoir pressure with depth at the well location for all three cases at the end time for the Homogeneous Shallow model for Run A*

To understand the differences between the flow rates based on the distance to the impermeable boundary, a more thorough look at the underlying parameters is necessary. The first parameter to look at when analyzing the total flow rate results is the reservoir pressure. Figure 18 shows the initial reservoir pressure, which is identical for all three cases, and the final reservoir pressure with depth at the well location for all three cases of the Homogeneous Shallow model. The location and thickness of the screened portion of the well is very clear from Figure 18 because it corresponds with the significant drop in pressure seen after 30 years of production. The well does impact the pressure in the upper and lower shale because the pressure is influenced below and above the screened section.

The total pressure decline in the reservoir at the end of the 30-year production period decreased slightly as the distance to the reservoir boundary increased. The higher pressure results in the higher flow rate in the well shown in Figure 12 where the flow rate for the cases is shown. Although the difference in pressure appears to be quite small, this difference for the entire volume of the reservoir can have a large impact.

The second parameter to analyze that influences the gaseous methane flow rate is the gas saturation in the reservoir. Figure 19 shows the gas saturation, the pore volume filled with gas, after 30 years of production for all three cases for the Homogenous Shallow model along the y-axis at the midpoint of the screened portion of the well. The initial gas saturation is 1% at all depths. The gas saturation along the y-axis is very similar between the three cases except within 50 m from the well. At this point the gas saturation for Case 2 and Case 3 after the 30 years of production is slightly higher than for Case 1. The graph only shows the gas saturation above 5% which corresponds with the percentage that is mobile and not trapped in the pore space. At greater than 83 m away from the well, all the gas is trapped in the pore space and is not mobile. The gas saturation for Case 2 farther from the well is slightly different due to a difference in grid cell spacing and the impact of this on the simulation results.

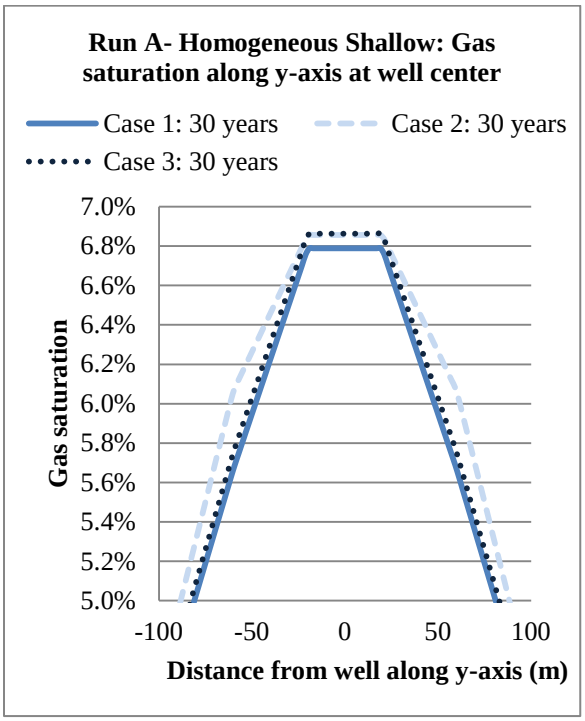


*Figure 19: Gas saturation with distance from the well along the y-axis at the center of the screened section for all three cases at the end time for the Homogeneous Shallow model for Run A*

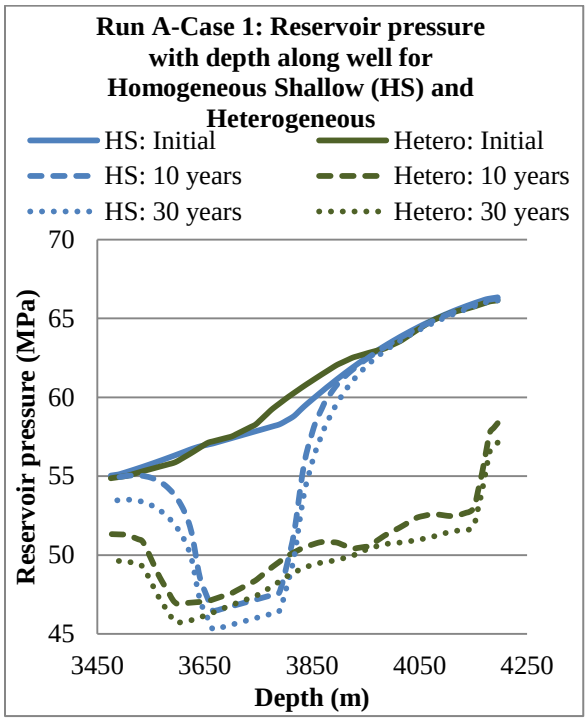


*Figure 20: Reservoir pressure with depth along the well for Case 1 for the Homogeneous Shallow and Heterogeneous models*

For each sandstone layer in the Heterogeneous model, the pressure drops significantly over time with the well production. This is similar to what happens for the single layer with the Homogeneous model. However, because the drop in pressure from the well in the screened portion also influences the upper and lower boundary layers, the pressure drop throughout the entire reservoir thickness is much greater for the heterogeneous model than for the homogeneous models. After a significant period of time the reservoir pressure in the Heterogeneous model has declined a similar amount for both the shale and sandstone layers influenced by the well.

Figure 20 shows the comparison for Case 1 for the reservoir pressure with depth between the Heterogeneous and the Homogeneous Shallow at the well location. The reservoir pressure is shown at the initial time, after approximately 10 years of production, and at the end of the production period of 30 years. At 10 years for the Heterogeneous model, the pressure drop is greater in the bottom two sandstone layers than in the shale. However, by 30 years, the reservoir pressure has declined a similar amount from the initial reservoir pressure between the top of the upper sandstone to the bottom of the lowest sandstone layer.

The significant overall drop in pressure over a large portion of the reservoir in the Heterogeneous model explains why the flow rates for the Heterogeneous models are so much higher than for both of the homogeneous models. The pressure drops in the bounding shale layers due to fluid leakage from these layers into the sandstone layers during production. Farther away from the well the resultant pressure drop in the shale layers becomes significantly lower than the pressure drop seen at the same location in the sandstone layers as shown in Figure 21. The black dashed lines on Figure 21 show the location of the sandstone layers and the depth to the top of the sandstone layers is listed in Table 6.

*Table 6: Depth to the top of the sandstone layers*

| Layer | Sand/Shale | Depth to top (m) |
|---|---|---|
| Layer 1 | Sand | 3565 |
| Layer 3 | Sand | 3700 |
| Layer 5 | Sand | 3985 |
| Layer 7 | Sand | 4120 |

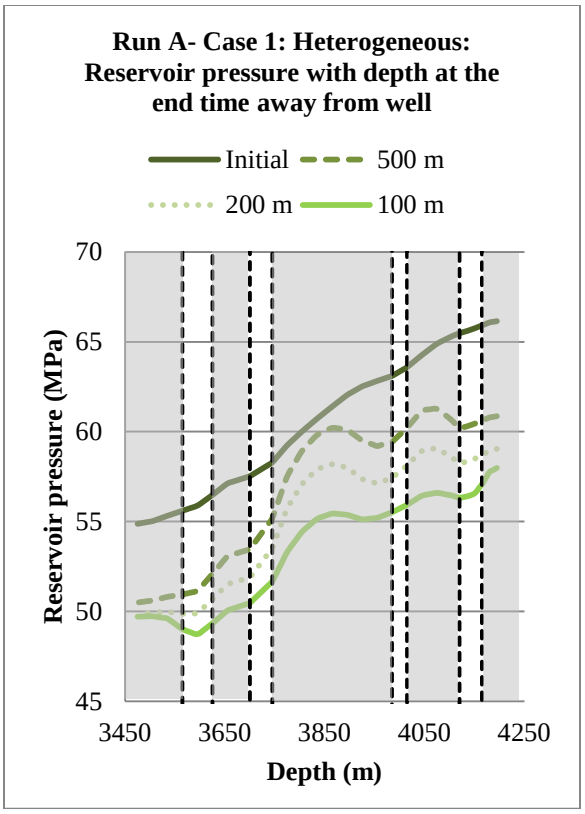


*Figure 21: Reservoir pressure with depth at the end time for Case 1 with the Heterogeneous model at 100 m, 200 m, and 500 m away from well along y-axis (shale is gray)*

Layer 4, which is comprised entirely of low permeability shale, shows the lowest pressure drop of all the layers moving farther away from the well. At 500 m away from the well the pressure in Layer 4 is close to the initial pressure in the reservoir. The pressure drop moving farther away from the well is still the highest at the top and bottom of the reservoir where the majority of the producing sandstone is located.

## CONCLUSIONS

This work is an initial look at the influence of upscaling from a model with multiple layers of sandstone and shale based on a well log to a three layer model on the fluid and methane production from a geopressured geothermal reservoir. Combining the four sandstone layers into one homogeneous layer significantly impacts both the total flow rate and the gaseous methane flow rate results. In all cases, the Heterogeneous model had the highest total flow at any point during the production period. The main reason for the higher total flow rate is due to the much greater pressure drop throughout the majority of the reservoir interval that occurs during production in the Heterogeneous model. With a higher total flow rate there is more heat recovered from the reservoir. Additionally, the production of methane from the Heterogeneous model is significantly higher than the Homogeneous Shallow model that has a similar initial pressure differential. The total methane produced ranges from 16.4 BCF to 17.0 BCF over the thirty year period. This methane could be burned on site to produce electricity or sold to the market. The results suggest that a simplified model that combines multiple layers of sandstone into a single layer gives a reasonable, although conservative, estimate of the recoverable geopressured geothermal resource.

The pressure difference between the well and the reservoir was found to have a large impact on the model results. For Run A with the pressure at the top of the screened well section equal between the three reservoir models at 40 MPa, the difference in flow rate between the three models is quite large. This is true even though the pressure in the sandstone intervals at the end time is quite similar for Run A. However, the drop in pressure has the greatest impact on flow rate. For Run B where the well head pressure for the Homogeneous Shallow and Heterogeneous models is the same at 3.0 MPa, the difference between the flow rates is greater because the initial pressure differential for the Homogeneous Shallow model is reduced. For the same well head pressure the allowance for frictional pressure loss is the same. For Run C where the initial pressure differential is the same at 16.9 MPa for the Homogeneous Shallow and the Homogeneous Deep, the difference in flow rates is very small. However, if the sandstone is placed at a greater depth such as in Homogeneous Deep, then a larger pressure differential is possible with the same allowance for frictional pressure loss in the well. The results indicate that the assumptions used to determine the production pressure profile in the well must be considered when comparing results among simulations.

Finally, the influence of the distance to the impermeable boundary is clear in both the Homogeneous Shallow model and the Heterogeneous model. The influence is greater in the Homogeneous Shallow model than in the Heterogeneous model because the boundaries have a greater influence on the pressure in the single layer. The change in reservoir volume impacts the total flow rate less than it does the gaseous methane flow rate. It can be hard to determine the distance from impermeable boundaries for a reservoir based on available reservoir data. Data from multiple well logs as well as seismic data can help to identify flow barriers. Since the distance to the boundary does have an impact on both the Heterogeneous and the

Homogeneous Shallow models, it is a parameter that should be determined before production begins.

## REFERENCES


Battistelli A., Calore, C. and Pruess, K. (1997), "The simulator TOUGH2/EWASG for modelling geothermal reservoirs with brines and non-condensible gas," *Geothermics*, **26**, 437-464.

Bebout, D. G., Weise, B. R., Gregory, A. R. and Edwards, M. B. (1982), "Wilcox sandstone reservoirs in the deep subsurface along the Texas Gulf Coast: their potential for production of geopressured geothermal energy," Report of Investigations No. 117. Texas Univ., Austin, Bureau of Economic Geology.

Bebout D. G., Loucks, R. and Gregory, A. R. (1983), "Frio sandstone reservoirs in the deep subsurface along the Texas Gulf Coast: their potential for production of geopressured geothermal energy," Texas Univ., Austin, Bureau of Economic Geology.

Coats, K. H. (1977), "Geothermal Reservoir Modeling," Society of Petroleum Engineers-6892. 52nd Annual Fall Technical Conference and Exhibition of the SPE, Denver, Colorado.

Gregory, A. R., Dodge, M., Posey, J. and Morton, R. (1980), "Volume and accessibility of entrained (solution) methane in deep geopressured reservoirs-tertiary formations of the Texas Gulf Coast," Final report, Texas Univ., Austin, Bureau of Economic Geology.

Loucks, R. G., Dodge, M. M. and Galloway, W. E. (1979), "Sandstone consolidation analysis to delineate areas of high-quality reservoirs suitable for production of geopressured geothermal energy along the Texas Gulf Coast," Final Report, Texas Univ., Austin, Bureau of Economic Geology.

Papadopulos S., Wallace Jr, R., Wesselman, J., and Taylor, R. (1975), "Assessment of onshore geopressured-geothermal resources in the northern Gulf of Mexico basin," US Geological Survey, Circular 726, 125-146.

Pruess K., Oldenburg, C., and Moridis, G. (1999), "TOUGH2 User's Guide Version 2.0," Berkeley, California. Lawrence Berkeley National Labs Report LBNL-43134, Earth Science Division, University of California, Berkeley.

Riney, T. D. (1988), "Gladys McCall Geopressured Reservoir Analysis," *Energy Resources Technology*, **110**, 262-268.

Riney, T. D. (1991), "Pleasant Bayou Geopressured-Geothermal Reservoir Analysis," *Energy Resources Technology*, **114**, 315-322.

Schowalter, T. T, and Hess, P. D (1982), "Interpretation of Subsurface Hydrocarbon Shows," *AAPG Bulletin*, **66,** 1302-1327

Wallace, R., Kraemer, T., Taylor, R., and Wesselman, J. (1978), "Assessment of geopressured-geothermal resources in the northern Gulf of Mexico basin." US Geological Survey, Circular 790, 132–155.

Warren, J. E. and Price, H.S. (1961), "Flow in heterogeneous porous media," *Society of Petroleum Engineers Journal*, **1**, 153–169.

Weber, K.J. and van Geuns, L. C. (1990), "Framework for constructing clastic reservoir simulation models," *Journal of Petroleum Technology*, **42**, 1248–1253.

Yale, D.P., Nabor, G.W., Russell, J.A., Pham, H.D., and Yousef, M. (1993) "Application of Variable Formation Compressibility for Improved Reservoir Analysis," 68th Annual Technical Conference and Exhibition of the SPE, Houston, Texas.